Supplement of Atmos. Chem. Phys., 22, 12207–12220, 2022
https://doi.org/10.5194/acp-22-12207-2022-supplement

Atmospheric Chemistry and Physics
Open Access
EGU

Supplement of

The effect of COVID-19 restrictions on atmospheric new particle formation in Beijing

Chao Yan et al.

Correspondence to: Markku Kulmala (markku.kulmala@helsinki.fi), Jingkun Jiang (jiangjk@tsinghua.edu.cn) and Aijun Ding (dingaj@nju.edu.cn)

1. Calculation of condensation sink, particle formation rate, growth rate, and survival probability

The condensation sink of H_2SO_4 was calculated by Eq.1 as shown below (Kulmala et al., 2012).

$$CS = 2\pi D_v \int_0^{d_{p,max}} d_p \beta n(d_p) dd_p$$

Where, d_p is particle diameter measured by the combination of DEG-SMPS and PSD; β is transitional correction factor for mass flux; $n(d_p)$ is the number concentration of particles of diameter d_p; D_v is diffusion coefficient of H_2SO_4.

Particle formation rates at 1.5 nm ($J_{1.5}$) are calculated based on measurement by DEG-SMPS. The calculation is based on the balanced formula that improves the estimation of particle losses due to coagulation scavenging in the polluted urban atmosphere (Cai and Jiang, 2017),

$$J_k = \frac{dN_{[d_k,d_u]}}{d_t} + \sum_{d_g=d_k}^{d_{u-1}} \sum_{d_i=d_{min}}^{+\infty} \beta_{(i,g)} N_{[d_i,d_{i+1}]} N_{[d_g,d_{g+1}]} - \frac{1}{2} \sum_{d_g=d_{min}}^{d_{u-1}} \sum_{d_i^3=max(d_{min}^3, d_k^3-d_{min}^3)}^{d_{i+1}^3+d_{g+1}^3 \le d_u^3} \beta_{(i,g)} N_{[d_i,d_{i+1}]} N_{[d_g,d_{g+1}]} + n_u \cdot GR_u$$

where J_k is the formation rate of particles at size d_k, N is the particle number concentration, and $N_{[dk;du]}$ is defined as the total number concentration of particles in the size range from d_k to d_u (particles with diameters of du are not accounted for); d_i refers to the lower bound of each measured size bin; $\beta_{(i,g)}$ is the coagulation coefficient when particles with the diameter d_i collide with particles with the diameter d_g; n is the particle size distribution function that equals dN/dd_p; GR_u is the particle growth rate at d_u, i.e., dd_u/dt; and d_u is the upper bound of the size range for calculation. The size of the minimum cluster in theory and the lowest size limit of the measuring instrument in practice is represented by d_{min}. On the righthand side of the equation, the first term is called dN/dt term; the second minus the third term together is the coagulation term, and the last term is the condensational growth term.

For the calculation of $J_{1.5}$ based on DEG-SMPS data, d_k is 1.5 nm and d_{min} is 1.3 nm. We have also tested different upper size for d_u of 3 nm and 25 nm in $J_{1.5}$ calculation, and results show no discrepancy during the strong NPF cases. Thus, d_u is set to 3 nm in order to avoid the potential influence of primary vehicle emission or transport of nucleation mode particles on the dN/dt term.

Growth rates (GR) is calculated based on the appearance time method, where the appearance time of maximum is automatically fitted by Gaussian curve for the particle of each size bin. We calculate the size-segregated GR in three size ranges, i.e., 1.5 – 3 nm (GR_{1-3}), 3 – 7 nm

($GR_{3\text{-}7}$), and 7 – 15 nm ($GR_{7\text{-}15}$). $GR_{3\text{-}7}$ is used in the calculation of $J_{1.5}$, and it accounts for only about 10% of the J values, which also means that the error in GR is not important for $J_{1.5}$ determination.

The survival probability for particles over a certain size range (dp_1, dp_2) was calculated as the difference in formation rate between the upper and lower bound $SP=J_{dp2}/J_{dp1}$. We used the daily maximum of measured formation rate for the calculation of the survival probability. In contrast to this, we also estimated the theoretical survival probability from the Kerminen & Kulmala equation (Kerminen and Kulmala, 2003), which relates the formation rate at a smaller size dp_1 to the formation rate at a larger size dp_2 via $J_{dp1} = J_{dp2}\ \exp(0.23\times\ (1/dp_1 - 1/dp_2)\ CS'/GR_{dp1\text{-}dp2})$ with $CS' \sim 1\times10^4$ CS in [s^{-1}] and GR in [nm h^{-1}]. As the survival probability is defined as the ratio of the two formation rates, we obtain for the theoretical survival estimate from the measured GR and CS: $SP=J_{dp2}/J_{dp1}=\exp(-0.23\times(1/dp_1 - 1/dp_2)\ \times CS'/GR_{\ dp1\text{-}dp2})$.

2. Estimation of OOM Volatility

Detailed structure information of OOMs in real atmosphere is still unknown, therefore, the volatility of each OOM molecule was estimated based on a parameterization using numbers of different atoms [1]. For the oxidation products from monoterpenes, previous studies show that except from hydroxyl (-OH), carbonyl (-C=O) and carboxyl (-C(O)OH) groups, hydroperoxide (-OOH) also takes a large portion [2, 3]. Then by assuming that all nitrogen atoms exist as organonitrate groups ($-ONO_2$), the saturation mass concentration of OOM molecule at 300 K can be given as follows [2]:

$$\log_{10}C^*(300\mathrm{K}) = (25 - \mathrm{nC})\cdot \mathrm{bC} - (\mathrm{nO} - 3\mathrm{nN})\cdot \mathrm{bO} - 2 * \left[\frac{(\mathrm{nO} - 3\mathrm{nN})\cdot \mathrm{nC}}{\mathrm{nC} + \mathrm{nO} - 3\mathrm{nN}}\right]\cdot \mathrm{bCO} - \mathrm{nN}\cdot \mathrm{bN}$$

where nC, nO and nN are the numbers of carbon, oxygen, and nitrogen in each molecule respectively, and bC=0.475, bO=0.2, bCO=0.9, and bN=2.5. For oxidation products from aromatics, the work of Mingyi Wang et al. shows that they possess more -OH and -C=O groups as well as less hydroperoxides, and that their estimated saturation concentrations suggested by Donahue et al. [1] match well with the experiment ones [4]. Therefore, for those non-monoterpene OOMs, the estimation from Donahue et al. was applied:

$$\log_{10}C^*(300\mathrm{K}) = (25 - \mathrm{nC})\cdot \mathrm{bC} - \mathrm{nO_{eff}}\cdot \mathrm{bO} - 2 * \left(\frac{\mathrm{nC}\cdot \mathrm{nO_{eff}}}{\mathrm{nC} + \mathrm{nO_{eff}}}\right)\cdot \mathrm{bCO}$$

where nC, nO_{eff} and nN are the numbers of carbon, effective oxygen and nitrogen in each molecule separately, and bC=0.475, bO=2.3, and bCO=-0.3.

The temperature dependence of C^* is given by the Clausius-Clapeyron equation [5, 6], which we can be approximated as:

$$\log_{10}C^*(\mathrm{T}) = \log_{10}C^*(300\mathrm{K}) + \frac{\Delta H_{vap}}{R\ln(10)}\left(\frac{1}{300} - \frac{1}{T}\right)$$

where the evaporation enthalpy ΔH_{vap} can be linked with $\log_{10}C^*(300\mathrm{K})$ according to the following equation:

$$\Delta H_{vap}[\mathrm{kJ\ mol^{-1}}] = -5.7\cdot \log_{10}C^*(300\mathrm{K}) + 129$$

After the temperature related saturation concentrations were calculated, OOMs were then grouped into different bins based on the volatility basis set (VBS) [7], and further classified as ELVOCs (extremely low volatility organic compounds), LVOCs (low volatility organic compounds), SVOCs (semi-volatile organic compounds), IVOCs (intermediate volatility organic compounds) and VOCs (volatile organic compounds) according to their volatilities [6].

3. Estimation of particle growth rate by OOM condensation

3.1 Non-volatile particle growth model

The contribution of OOMs to particle growth rate was calculated using a non-volatile particle growth model. The equations are shown below[8]:

$$GR = \gamma \frac{m_v}{2\rho_v}\left(\frac{8kT}{\pi m_v}\right)^{\frac{1}{2}}\left(1+\frac{d_v}{d_p}\right)^2 OOM_{cond} \quad \gamma = \frac{4}{3}Kn\beta_m$$

Here, where m_v, d_v, ρ_v, and OOM_{cond} are the molecular mass, diameter, condensed-phase density, and concentration of condensable OOMs, respectively. Kn is the Knudsen number and β_m is the Fuchs-Sutugin transition regime correction factor for mass flux. For OOMs, m_v is directly measured as the mass-to-charge ratio of OOMs, and ρ_v and d_v are assumed as constants of 1.5 g cm^{-3} and 0.9 nm, respectively[9].

The nitrate CI-APi-LTOF measures OOMs with a wide volatility range (Figure S8), yet only low-volatility ones are able to condense onto the particle surface. In a previous chamber experiment[2], it was shown that OOMs classified as LVOC and ELVOC, i.e., $\log_{10}(C^*) \leq -0.5$, dominate the particle growth at a size below 30 nm almost irreversibly, while SVOC OOMs are not able to efficiently condense. Therefore, OOM_{cond} in this study is the total concentration of ULVOC, ELVOC and LVOC.

3.2 Tuning on OOM concentration

In the aforementioned chamber study[2], it was also suggested that nitrate CI-APi-TOF might underestimate LVOC OOM concentration, as those observed particle growth rates could be only simulated with a scaled OOM concentration. Later on, studies demonstrated that this was due to the declined charging efficiency for OOMs with relatively low oxygen-to-carbon ratios (O/C)[10] and insufficient hydrogen-donating functional groups[11]. To account for this possible underestimation of OOM concentration, we scaled OOM concentration by multiplying OOMs with O/C of 6, 5, 4, and 3 by a factor of 2, 4, 10, and 10, respectively. These factors are the same as those have been used in the chamber study[2]. It must be noted that, such scaling should be considered arbitrary, which may not reflect the actual underestimation. However, with such scaled OOMs, we were able to better explain the observed particle growth rates (Figure S10), suggesting that OOM underestimation was one possible reason for the unexplained GR as shown in Figure 6.

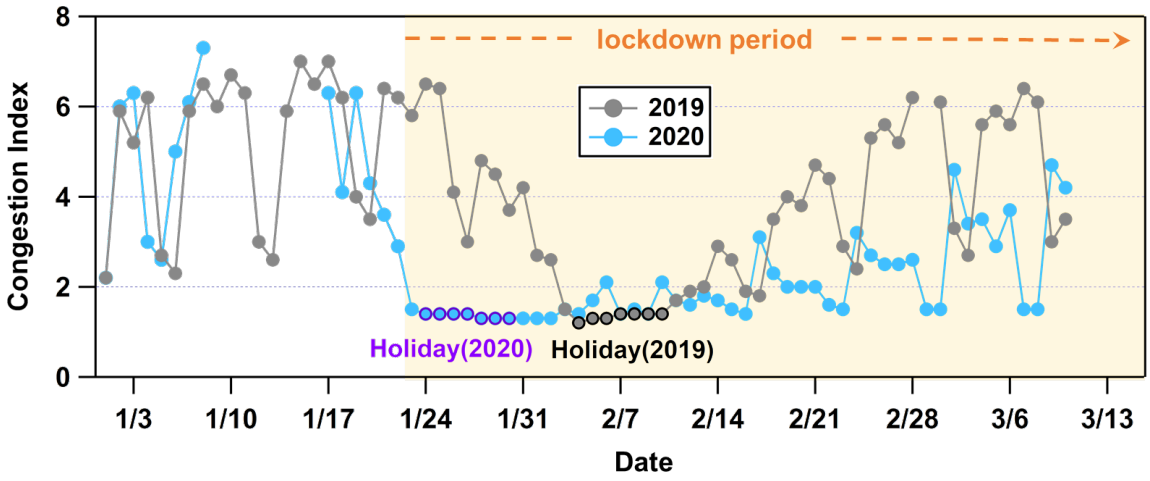

Figure S1. Traffic congestion index between 1st Jan to 10th Mar for 2019 and 2020. National holiday is marked as red for both 2019 (4th Feb – 10th Feb) and 2020 (24th Jan to 30th Jan). Yellow shaded area is the 'lockdown period' (24th Jan – 5th Mar, 2020) in this study.

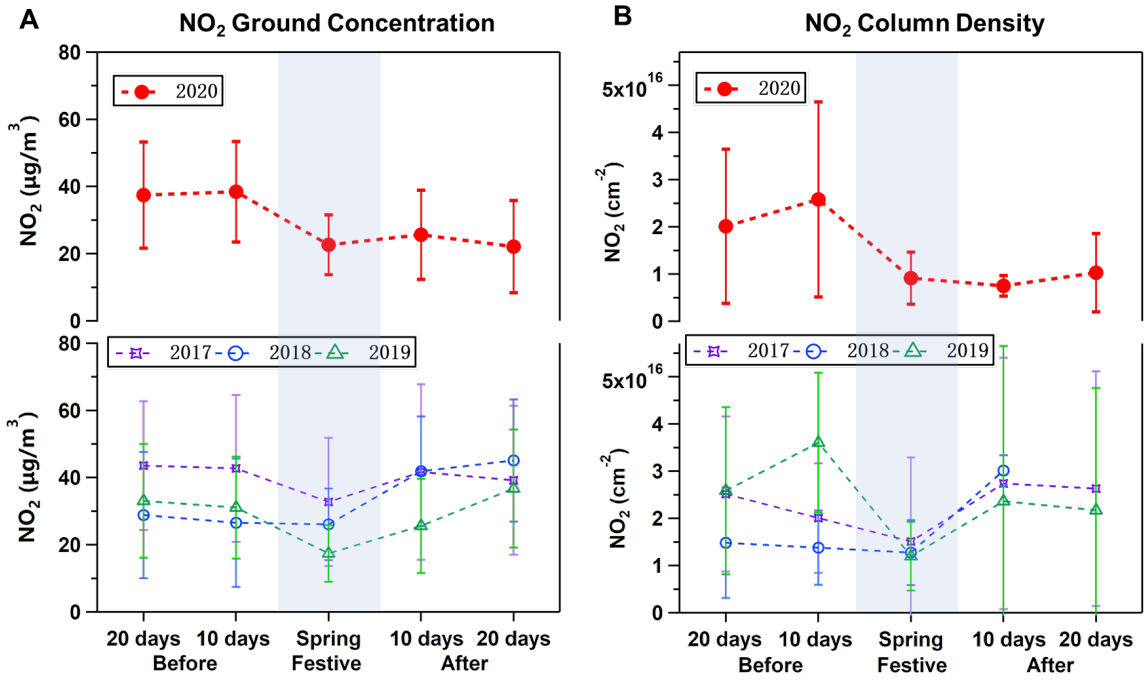

Figure S2. The trend of NO_2 in Beijing urban area around the Chinese Spring Festival of 2018, 2019 and 2020, a comparison between ground stations from the national monitoring network (a) and TROPOMI (b) data.

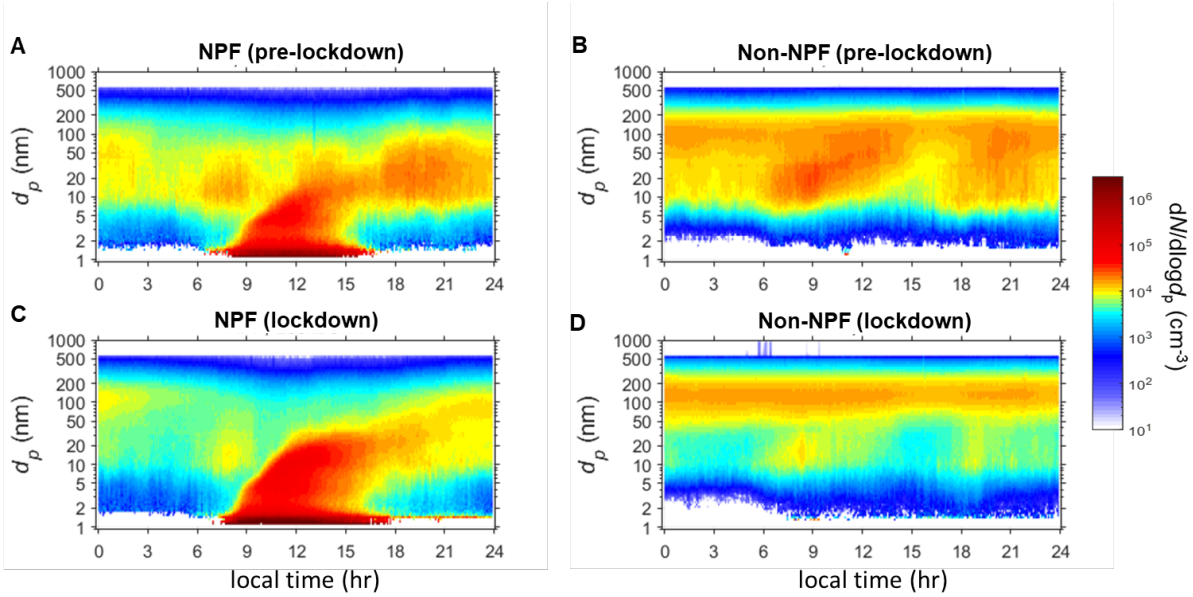

Figure S3. Particle number size distribution in NPF and non-event days during the pre-lockdown and lockdown periods.

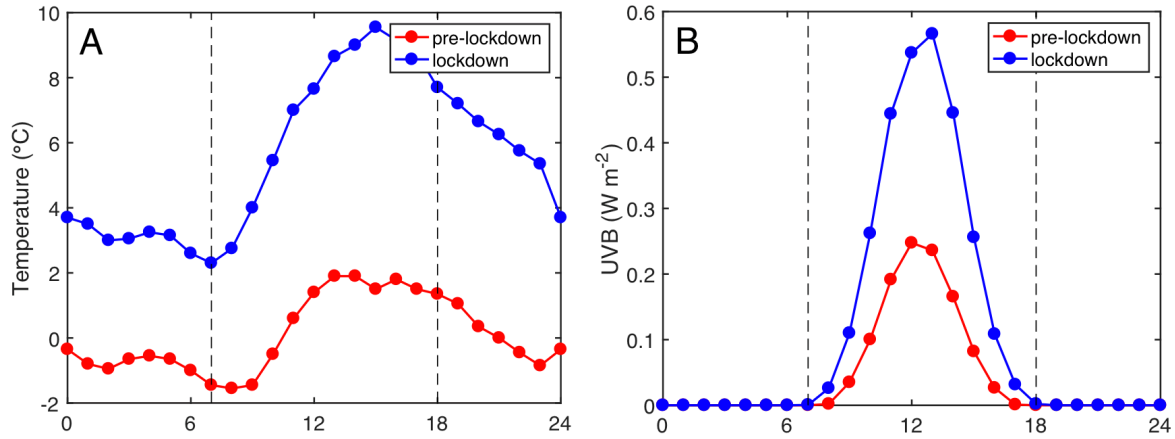

Figure S4. The diurnal patterns (median value) of temperature (A) and UVB (B) during the pre-lockdown and lockdown periods.

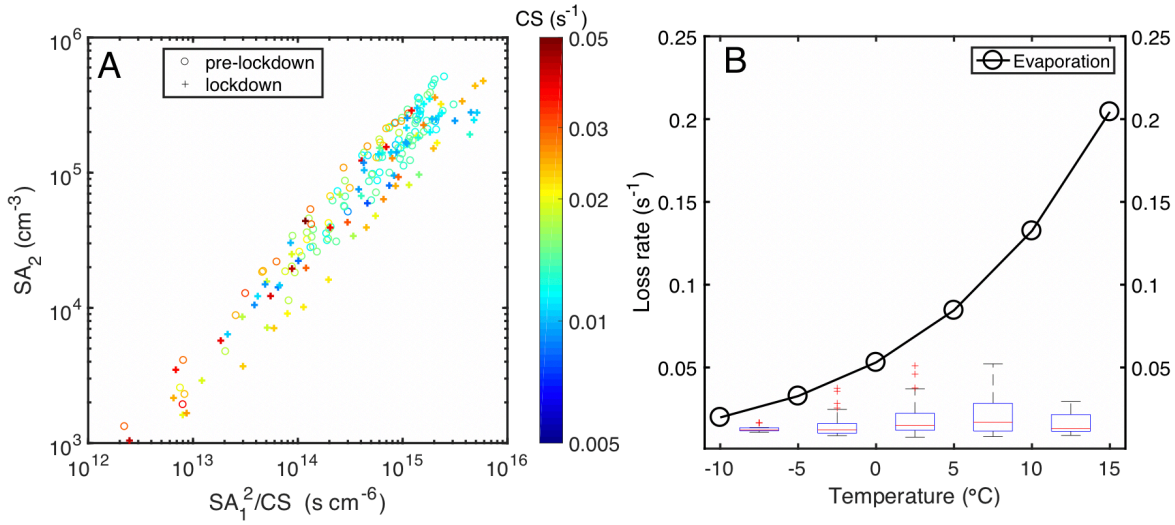

Figure S5. (A) SA clustering efficiency color-coded by CS. (B) The loss rate of SA_1-DMA_1 by evaporation and CS at different temperatures. The solid line with back circles denotes the loss due to evaporation, and the boxplots are the loss due to CS in respective temperature ranges.

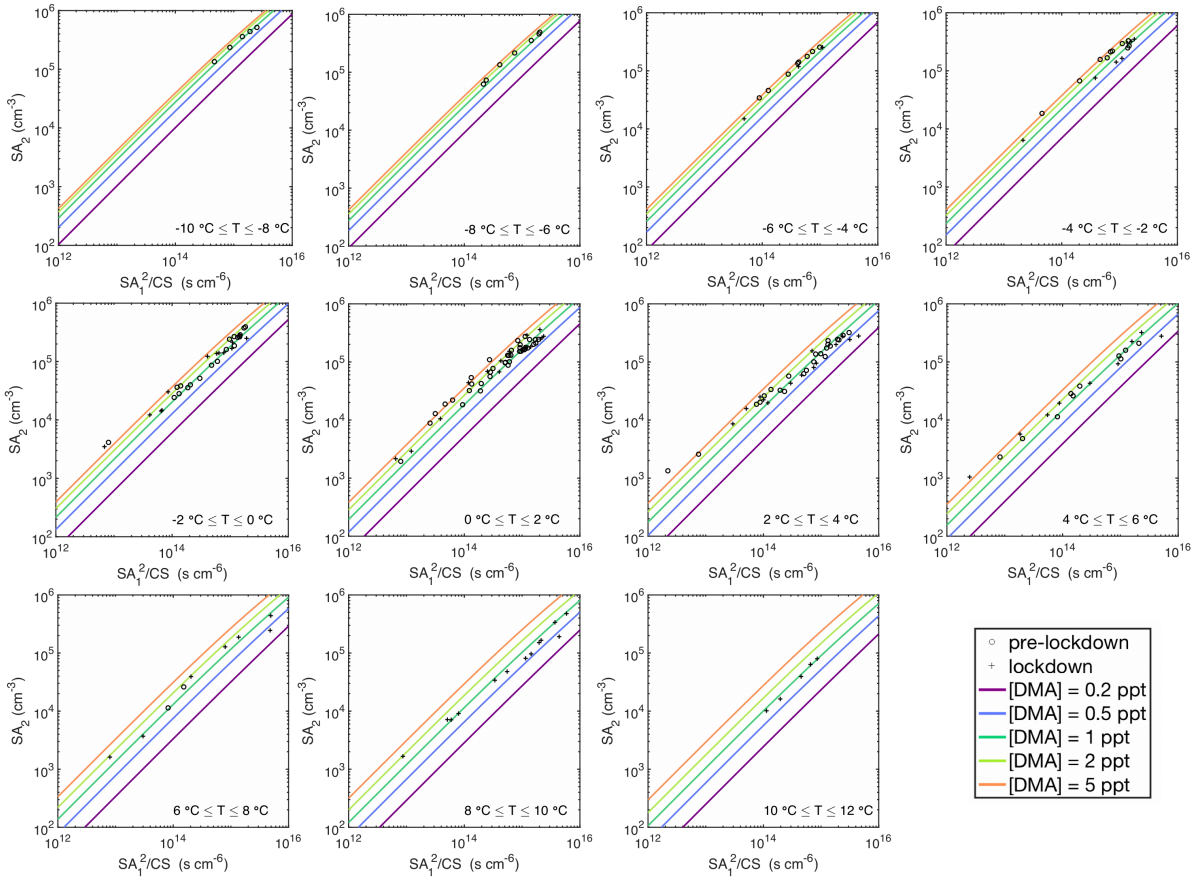

Figure S6. Simulations of SA_2 formation with various DMA concentrations and temperature ranges. It can be seen that most measured points locate between the lines representing a DMA concentration of 0.5 – 2 ppt. In addition, a systematic difference between pre-lockdown data and lockdown data can be clearly observed.

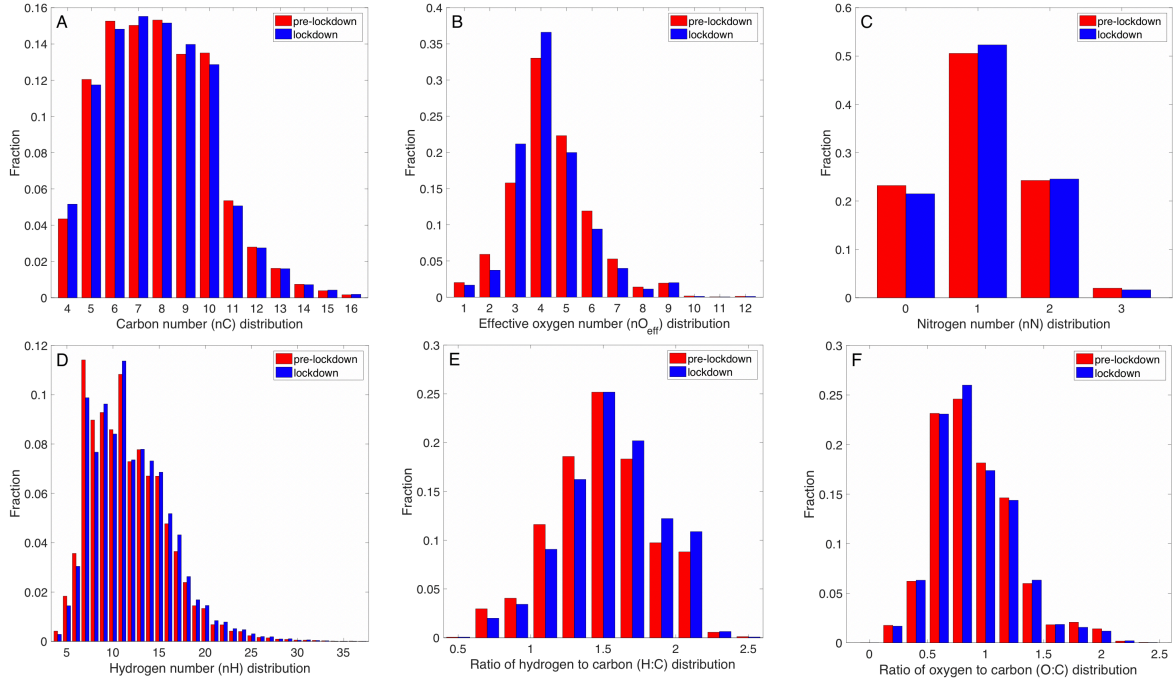

Figure S7. The distributions of carbon number, oxygen number, nitrogen number, hydrogen number, hydrogen-to-carbon ratio, and oxygen-to carbon ratio in the pre-lockdown and lockdown periods.

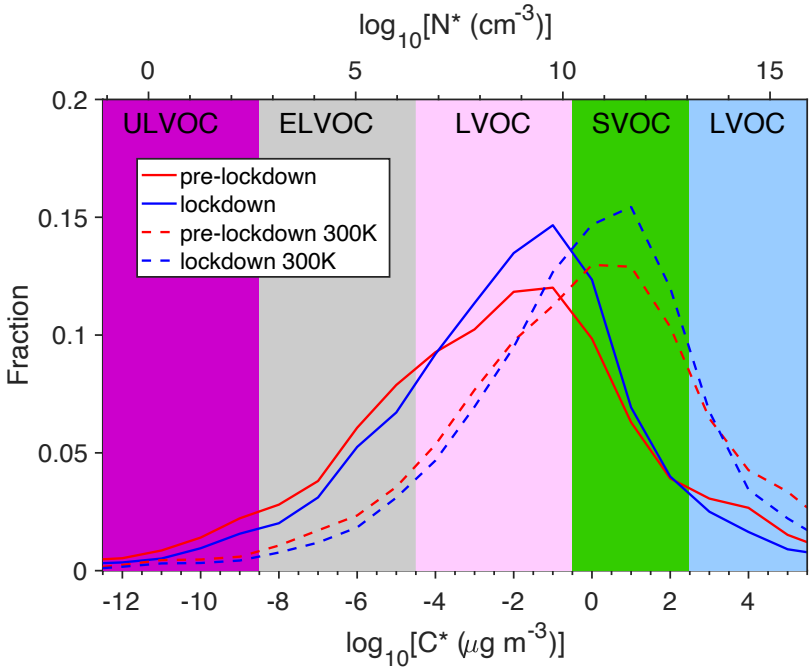

Figure S8. The "intrinsic" (300K) and real-temperature OOM volatility distribution during the pre-lockdown and lockdown periods. OOM volatility is binned according to its vapor pressure in the unit of μg m^{-3}. Another concentration unit of cm-3 is also provided assuming a mean OOM molar mass of 250 g mol^{-1}.

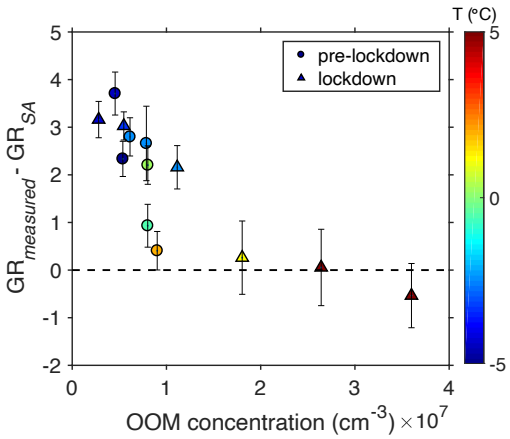

Figure S9. The unexplained GR as a function of condensable OOM concentration. The measurement uncertainty (±50%) of SA is shown as the vertical error bars. Data points are color-coded with the mean temperature at the corresponding time window.

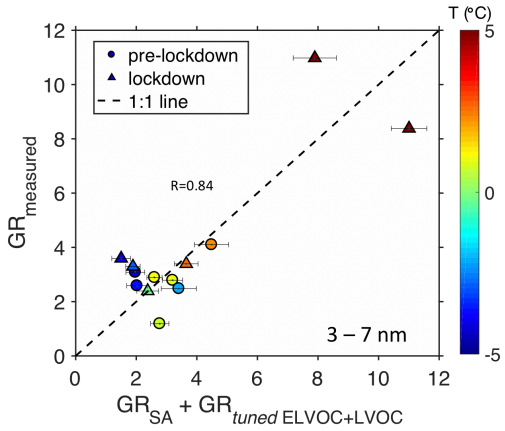

Figure S10. The relationship between measured GR_{3-7} and calculated GR_{3-7} based on a tuned OOM concentration. The measurement uncertainty (±50%) of SA is shown as the horizontal error bars. Data points are color-coded with the mean temperature at the corresponding time window.

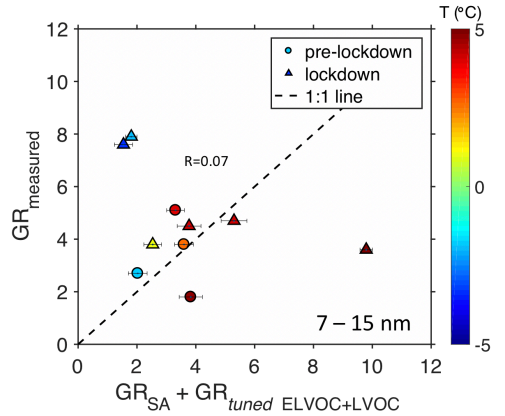

Figure S11. The relationship between measured GR_{7-15} and calculated GR_{7-15} based on a tuned OOM concentration. The measurement uncertainty (±50%) of SA is shown as the horizontal error bars. Data points are color-coded with the mean temperature at the corresponding time window.

1. Donahue, N. M.; Epstein, S. A.; Pandis, S. N.; Robinson, A. L., A two-dimensional volatility basis set: 1. organic-aerosol mixing thermodynamics. Atmospheric Chemistry and Physics **2011,** 11, (7), 3303-3318.

2. Tröstl, J.; Chuang, W. K.; Gordon, H.; Heinritzi, M.; Yan, C.; Molteni, U.; Ahlm, L.; Frege, C.; Bianchi, F.; Wagner, R.; Simon, M.; Lehtipalo, K.; Williamson, C.; Craven, J. S.; Duplissy, J.; Adamov, A.; Almeida, J.; Bernhammer, A.-K.; Breitenlechner, M.; Brilke, S.; Dias, A.; Ehrhart, S.; Flagan, R. C.; Franchin, A.; Fuchs, C.; Guida, R.; Gysel, M.; Hansel, A.; Hoyle, C. R.; Jokinen, T.; Junninen, H.; Kangasluoma, J.; Keskinen, H.; Kim, J.; Krapf, M.; Kürten, A.; Laaksonen, A.; Lawler, M.; Leiminger, M.; Mathot, S.; Möhler, O.; Nieminen, T.; Onnela, A.; Petäjä, T.; Piel, F. M.; Miettinen, P.; Rissanen, M. P.; Rondo, L.; Sarnela, N.; Schobesberger, S.; Sengupta, K.; Sipilä, M.; Smith, J. N.; Steiner, G.; Tomè, A.; Virtanen, A.; Wagner, A. C.; Weingartner, E.; Wimmer, D.; Winkler, P. M.; Ye, P.; Carslaw, K. S.; Curtius, J.; Dommen, J.; Kirkby, J.; Kulmala, M.; Riipinen, I.; Worsnop, D. R.; Donahue, N. M.; Baltensperger, U., The role of low-volatility organic compounds in initial particle growth in the atmosphere. Nature **2016,** *533*, (7604), 527-531.

3. Stolzenburg, D.; Fischer, L.; Vogel, A. L.; Heinritzi, M.; Schervish, M.; Simon, M.; Wagner, A. C.; Dada, L.; Ahonen, L. R.; Amorim, A.; Baccarini, A.; Bauer, P. S.; Baumgartner, B.; Bergen, A.; Bianchi, F.; Breitenlechner, M.; Brilke, S.; Buenrostro Mazon, S.; Chen, D.;

Dias, A.; Draper, D. C.; Duplissy, J.; El Haddad, I.; Finkenzeller, H.; Frege, C.; Fuchs, C.; Garmash, O.; Gordon, H.; He, X.; Helm, J.; Hofbauer, V.; Hoyle, C. R.; Kim, C.; Kirkby, J.; Kontkanen, J.; Kürten, A.; Lampilahti, J.; Lawler, M.; Lehtipalo, K.; Leiminger, M.; Mai, H.; Mathot, S.; Mentler, B.; Molteni, U.; Nie, W.; Nieminen, T.; Nowak, J. B.; Ojdanic, A.; Onnela, A.; Passananti, M.; Petäjä, T.; Quéléver, L. L. J.; Rissanen, M. P.; Sarnela, N.; Schallhart, S.; Tauber, C.; Tomé, A.; Wagner, R.; Wang, M.; Weitz, L.; Wimmer, D.; Xiao, M.; Yan, C.; Ye, P.; Zha, Q.; Baltensperger, U.; Curtius, J.; Dommen, J.; Flagan, R. C.; Kulmala, M.; Smith, J. N.; Worsnop, D. R.; Hansel, A.; Donahue, N. M.; Winkler, P. M., Rapid growth of organic aerosol nanoparticles over a wide tropospheric temperature range. Proceedings of the National Academy of Sciences U S A **2018,** 115, (37), 9122.

4. Wang, M.; Chen, D.; Xiao, M.; Ye, Q.; Stolzenburg, D.; Hofbauer, V.; Ye, P.; Vogel, A. L.; Mauldin, R. L.; Amorim, A.; Baccarini, A.; Baumgartner, B.; Brilke, S.; Dada, L.; Dias, A.; Duplissy, J.; Finkenzeller, H.; Garmash, O.; He, X.-C.; Hoyle, C. R.; Kim, C.; Kvashnin, A.; Lehtipalo, K.; Fischer, L.; Molteni, U.; Petäjä, T.; Pospisilova, V.; Quéléver, L. L. J.; Rissanen, M.; Simon, M.; Tauber, C.; Tomé, A.; Wagner, A. C.; Weitz, L.; Volkamer, R.; Winkler, P. M.; Kirkby, J.; Worsnop, D. R.; Kulmala, M.; Baltensperger, U.; Dommen, J.; El-Haddad, I.; Donahue, N. M., Photo-oxidation of Aromatic Hydrocarbons Produces Low-Volatility Organic Compounds. Environmental Science & Technology **2020,** *54*, (13), 7911-7921.

5. Epstein, S. A.; Riipinen, I.; Donahue, N. M., A Semiempirical Correlation between Enthalpy of Vaporization and Saturation Concentration for Organic Aerosol. Environmental Science & Technology **2010,** 44, (2), 743-748.

6. Donahue, N. M.; Kroll, J. H.; Pandis, S. N.; Robinson, A. L., A two-dimensional volatility basis set – Part 2: Diagnostics of organic-aerosol evolution. Atmospheric Chemistry and Physics **2012,** 12, (2), 615-634.

7. Donahue, N. M.; Robinson, A. L.; Stanier, C. O.; Pandis, S. N., Coupled Partitioning, Dilution, and Chemical Aging of Semivolatile Organics. Environmental Science & Technology **2006,** 40, (8), 2635-2643.

8. Nieminen, T.; Lehtinen, K. E. J.; Kulmala, M., Sub-10 nm particle growth by vapor condensation – effects of vapor molecule size and particle thermal speed. Atmospheric Chemistry and Physics **2010,** 10, (20), 9773-9779.

9. Ehn, M.; Thornton, J. A.; Kleist, E.; Sipila, M.; Junninen, H.; Pullinen, I.; Springer, M.; Rubach, F.; Tillmann, R.; Lee, B.; Lopez-Hilfiker, F.; Andres, S.; Acir, I. H.; Rissanen, M.; Jokinen, T.; Schobesberger, S.; Kangasluoma, J.; Kontkanen, J.; Nieminen, T.; Kurten, T.; Nielsen, L. B.; Jorgensen, S.; Kjaergaard, H. G.; Canagaratna, M.; Maso, M. D.; Berndt, T.; Petaja, T.; Wahner, A.; Kerminen, V. M.; Kulmala, M.; Worsnop, D. R.; Wildt, J.; Mentel, T. F., A large source of low-volatility secondary organic aerosol. Nature **2014,** *506*, (7489), 476-9.

10. Riva, M.; Rantala, P.; Krechmer, J. E.; Peräkylä, O.; Zhang, Y.; Heikkinen, L.; Garmash, O.; Yan, C.; Kulmala, M.; Worsnop, D.; Ehn, M., Evaluating the performance of five different chemical ionization techniques for detecting gaseous oxygenated organic species. Atmospheric Measurement Techniques **2019,** *12*, (4), 2403-2421.

11. Hyttinen, N.; Kupiainen-Maatta, O.; Rissanen, M. P.; Muuronen, M.; Ehn, M.; Kurten, T., Modeling the Charging of Highly Oxidized Cyclohexene Ozonolysis Products Using Nitrate-Based Chemical Ionization. Journal of Physical Chemistry A **2015,** *119*, (24), 6339-45.